

Upconversion emission in near-stoichiometric LiNbO₃:Er³⁺ crystal

Cite this: *RSC Advances*, 2013, 3, 13507

Yannan Qian,^a Biao Wang,^{*a} Rui Wang,^{*b} Lili Xing^b and Yanling Xu^b

Important for increasing the efficiency of solar cells, multifunctional near-stoichiometric LiNbO₃ doped with Er³⁺ ions (Er:NSLN) could be considered as a luminescent layer to improve the solar spectrum response. The upconversion emission spectra show that Er:NSLN crystal converts the near infrared wavelength light which cannot be absorbed by the solar cells into the visible upconversion luminescence. The increased green and red upconversion emissions are observed in Er:NSLN crystal, and both green and red emitting states are populated by the three-photon process at the low pump power. As for the high pump power, the one-photon process is attributed to the "saturation" of the upconversion process. The Judd–Ofelt intensity parameters of Er:NSLN are calculated to be $\Omega_2 = 9.17 \times 10^{-20} \text{ cm}^2$, $\Omega_4 = 2.47 \times 10^{-20} \text{ cm}^2$ and $\Omega_6 = 1.00 \times 10^{-20} \text{ cm}^2$. Based on McCumber theory, the enhanced emission and absorption cross-sections of the green and red emissions indicate that Er:NSLN used as the upconversion luminescent layer could emit high efficiency of visible luminescence re-absorbed by the solar cells.

Received 12th February 2013,
Accepted 16th May 2013

DOI: 10.1039/c3ra40744f

www.rsc.org/advances

1. Introduction

Solar energy is the most important renewable source for improving the global energy consumption and meeting the long-term worldwide energy demand.¹ To fill the gap left by fossil fuels, advances in the development of solar cells have been expanded since solar cells could use directly the energy radiated from the sun to generate the practicable heat or electricity.² However, absorbing only a part of the solar spectrum is the main limitation for the practical application of conventional solar cells.³ Amorphous silicon solar cell only absorbs the sunlight with wavelength shorter than 850 nm. Dye-sensitized solar cell has a high absorption in the visible range (400–700 nm), but its wide bandgap (1.7–1.8 eV) implies that the near infrared (NIR) solar radiation would be lost due to the transmission.⁴ Therefore, a strategy to enlarge the solar spectrum response by adding the luminescent layers on the solar cells has been reported.⁵ Upconversion (UC) is a luminescent process which could convert two or more low energy photons into one high energy photon which could be reabsorbed by the solar cell.⁶ Owing to the abundant energy levels, long lifetime excited states, narrow emission spectral lines and excellent chemical durability, rare earth ions can be easily populated by near-infrared radiation.⁷ Rare earth ions doped host materials, emitting the visible luminescence through absorbing the NIR or IR sunlight, have become the important building blocks for the upconverted luminescent

layers of the solar cell.^{6,8–13} Among the rare-earth ions, Er³⁺ ion has gained a tremendous amount of attention since its ⁴I_{15/2} → ⁴I_{11/2} transition matches the NIR wavelength of 980 nm.

Ferroelectric lithium niobate (LiNbO₃) crystal is an excellent material exhibiting diverse physical properties such as electro-optic, ferroelectric, piezo-electric and nonlinear optical properties.¹⁴ Furthermore, the studies on Er-doped LiNbO₃ (Er:LiNbO₃) for application in integrated optics^{15,16} are favorable for developing the miniaturization and integration of solar cells. The intrinsic defect antisites Nb_{Li}⁴⁺,¹⁷ forming as the Nb⁵⁺ ions locate in Li sites due to the lithium-deficient "congruent" composition ([Li]/[Nb] = 0.946), suppressing the properties of congruent LiNbO₃ (CLN). As the [Li]/[Nb] ratio approaches 1, the Nb_{Li}⁴⁺ content decreases in the near-stoichiometric LiNbO₃ (NSLN) crystal, and the structure of the crystal lattice is nearly perfect. NSLN crystal doped with Er³⁺ ions (Er:NSLN) could not only retain the inherent merits of the pure near-stoichiometric crystal, such as lower refractive index, larger electro-optic and nonlinear optical effects, and remarkably lowered coercive field strength needed for ferroelectric domain reversal, but also show improvements in the optical properties of the Er³⁺ ion.¹⁸ To understand the spectral characteristics of the particular dopant–host combination, an accurate knowledge of absorption and emission cross-sections is required. To our knowledge, McCumber theory has been successfully applied to calculate the absorption and emission cross-sections.^{19–21} The effective parameters for the two thermalized ²H_{11/2} and ⁴S_{3/2} states are discussed in detail.

In this paper, near-stoichiometric LiNbO₃ heavily doped with Er³⁺ ions is grown by the Czochralski technique to gain the high fluorescent efficiency. A drastically enhanced red UC

^aSchool of Physics and engineering, Sun Yat-sen University, Guangzhou, 510275, China. E-mail: wangbiao@mail.sysu.edu.cn

^bDepartment of Chemistry, Harbin Institute of Technology, Harbin 150001, China. E-mail: wangrui001@hit.edu.cn

emission is observed in Er:NSLN crystal, and the UC mechanism is discussed. The Judd–Ofelt (J–O) intensity parameters Ω_t ($t = 2, 4$ and 6) and the spontaneous transition rate (A_{rad}) are calculated by J–O theory. McCumber theory is used to obtain the absorption and emission cross-sections for the visible upconversion emissions.

2. Experimental

Near-stoichiometric Er:LiNbO₃ crystal was grown along the ferroelectric c axis by the Czochralski technique from the melt with the [Li]/[Nb] molar ratio of 1. The molar fraction of the Er³⁺ ions in the melt was fixed at 3 mol%. As for a comparative study, congruent ([Li]/[Nb] = 0.946) LiNbO₃ crystal doped with 3 mol% Er³⁺ ions was also grown. The two crystals are named as Er:NSLN and Er:CLN, respectively. The raw materials (Li₂CO₃, Nb₂O₅ and Er₂O₃), whose purities were 99.99%, were fully ground in an agate mortar for 24 h. The Er:LiNbO₃ polycrystalline powders were formed *via* heat treatment of 750 °C for 2 h to remove CO₂, and then heating up to 1150 °C for 2 h. An axial temperature gradient of 40–50 K cm⁻¹, the rotating rate of 10–25 rpm and the pulling rate of 0.5–2 mm h⁻¹ were chosen to grow the crystals. The grown crystals were polarized at 1200 °C with a current density of 5 mA cm⁻². The boules were cut into Y-cut plates ($X \times Y \times Z = 10 \times 2 \times 10$ mm³) with carefully polished surfaces.

The inductively coupled plasma mass spectrometry (ICP-MS, Optima 7500 Series, Agilent Technologies Inc, Beijing) was used to determine the Er content ([Er³⁺]/[Nb⁵⁺] ratio) in the crystal. The ultraviolet-visible (UV-vis)-near infrared absorption spectrum was performed with unpolarized light and with a sample oriented in such a manner that the light propagated along the y axis of the crystal, and was recorded by a Perkin-Elmer Lambda-900 spectrophotometer. The scanning wavelength range was 310–1650 nm, and the scanning step and scanning speed were fixed at 1 nm and 600 nm min⁻¹, respectively. A power-controllable 980 nm diode laser was used to measure the UC emission spectra. All fluorescence emissions were recorded at the same geometry by using the spectrometer (Bruker optics 500IS/SM) equipped with a semiconductor cooled charge coupled device detector (DV440, Andor).

3. Results and discussion

Fig. 1 displays the UC emission spectra of Er:NSLN and Er:CLN crystals under 980 nm excitation. As illustrated in Fig. 1, the green and red UC emissions centered at 525/550 nm and 647 nm are observed, which correspond to the $^2\text{H}_{11/2}/^4\text{S}_{3/2} \rightarrow ^4\text{I}_{15/2}$ and $^4\text{F}_{9/2} \rightarrow ^4\text{I}_{15/2}$ transitions of Er³⁺ ion, respectively.²² It can be seen that the intensities of the green and red UC emissions in Er:NSLN are stronger than those in Er:CLN crystal, which will increase many more probabilities for practical applications of luminescent layers for the solar cell. The cross-section of solar cells with Er:NSLN luminescent layer may be designed

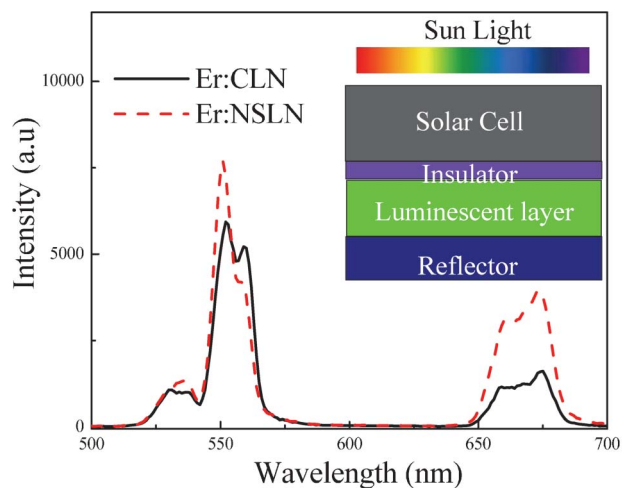


Fig. 1 The UC emission spectra of Er:NSLN and Er:CLN crystals under 980 nm excitation. The inset is the cross-section of solar cells with an Er:NSLN luminescent layer.

as the inset of Fig. 1. The Er:NSLN used as a luminescent layer is considered to be applied at the back of a solar cell combined with a back optical reflector. The Er:NSLN luminescent layer absorbs the NIR solar radiation and emits the visible green and red UC emissions which are subsequently reabsorbed by the solar cell.

In order to obtain the high efficiency of the green and red UC emissions, a better understanding of the UC mechanism is essential. Log–log plots of the intensity *versus* input pump power for the green and red UC emissions in Er:NSLN and Er:CLN crystals are displayed in Fig. 2. In general, for an unsaturated UC process, the number of photons required to

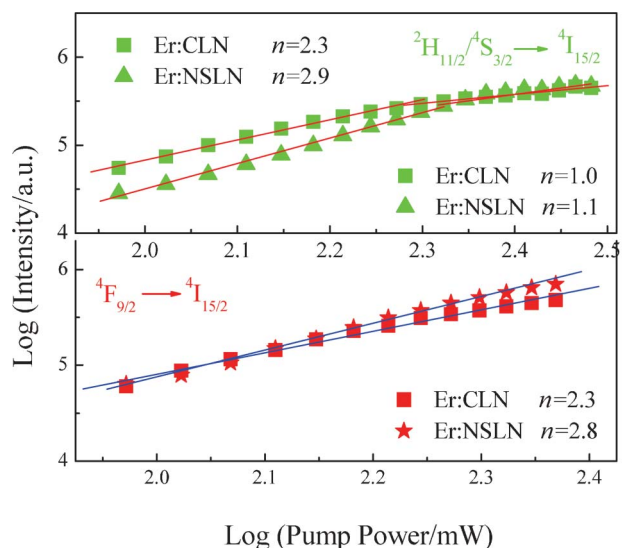


Fig. 2 The pump power dependences of the green and red UC emissions in Er:NSLN and Er:CLN crystals.

populate the upper emitting state can be obtained by the following equation:²³

$$I_f \propto P^n \quad (1)$$

where I_f is the output fluorescence intensity, P is the pump power, and n is the number required to populate the green and red UC emissions. As illustrated in Fig. 2, at the low pump power, the green and red UC emissions yield $n = 2.3$ and $n = 2.3$ in Er:CLN crystal, respectively. Although the n value of 2.3 deviates from the expected $n = 2$, only a two-photon process is considered as the UC mechanism to populate the $^4S_{3/2}/^2H_{11/2}$ and $^4F_{9/2}$ states in Er:CLN crystal. Here, the contribution of the green and red UC emissions populated *via* a three-photon process is neglected according to previous work. It has been found by S. K. Singh that the luminescence bands at 523 nm, 548 nm and 667 nm yield $n = 2.18$, 2.23 and 2.37, respectively, indicating that two incident near infrared photons are needed to produce these green and red luminescence bands in Er³⁺/Yb³⁺:Gd₂O₃ nanophosphor under 980 nm excitation.²⁴ A. H. Li has reported that the measured slope values of n are equal to 2.5, 2.3, 2.4 and 2.6 for the violet band at 410 nm, the green bands at 525 nm and 550 nm, and the red band at 660 nm, respectively, in Er:NSLN crystals. All these concerned UC emission bands are populated through the two-photon process under 800 nm excitation. The behavior that all slopes are close to 2.5 is attributed to the effect of self-focusing instead of cross relaxation process.²⁵ The studies on the optical characteristics of Er:LiNbO₃ crystals codoped without and with In³⁺ ions indicate that the n values of 2.2 and 2.3 are considered as the two-photon process involved in the UC mechanism responsible for populating the green emission in Er:LiNbO₃ crystals codoped with and without the In³⁺ ions.²⁶ Consequently, the two-photon process is only considered for populating the green and red UC emissions in the Er:CLN crystal here. In the case of the Er:NSLN crystal, the slope n values are observed to be 2.9 and 2.8 for the green and red UC emissions, respectively. This is an indication that three 980 nm photons are needed to populate the green and red emitting states in Er:NSLN crystal. It is worth noting that the slope n values for the green UC emission are nearly 1.0 at the high pump power.

The UC emission mechanisms of Er:NSLN and Er:CLN crystals under 980 nm excitation are shown in Fig. 3. At the low pump power, the two-photon process to populate the green and red UC emissions has been discussed in detail previously,^{27,28} which thereby is only briefly described as follows: Ground state absorption (GSA: $^4I_{15/2} + \text{a 980 nm photon} \rightarrow ^4I_{11/2}$) and excited state absorption (ESA1: $^4I_{11/2} + \text{a 980 nm photon} \rightarrow ^4F_{7/2}$) processes excite the Er³⁺ ions from the ground $^4I_{15/2}$ state to the $^4F_{7/2}$ state. Subsequently, the nonradiative relaxation from $^4F_{7/2}$ state populates the green emitting $^2H_{11/2}/^4S_{3/2}$ states. ESA3 ($^4I_{13/2} + \text{a 980 nm photon} \rightarrow ^4F_{9/2}$) is responsible for the population of the red emitting $^4F_{9/2}$ state. Due to the long lifetime of $^4I_{11/2}$ state, the cross relaxation (CR) processes (CR3: $^4I_{11/2} + ^4I_{11/2} \rightarrow ^4F_{7/2} + ^4I_{15/2}$ and CR4: $^4I_{13/2} + ^4I_{11/2} \rightarrow ^4F_{9/2} + ^4I_{15/2}$) may occur. As for the three-photon process for the green and red UC emissions, after

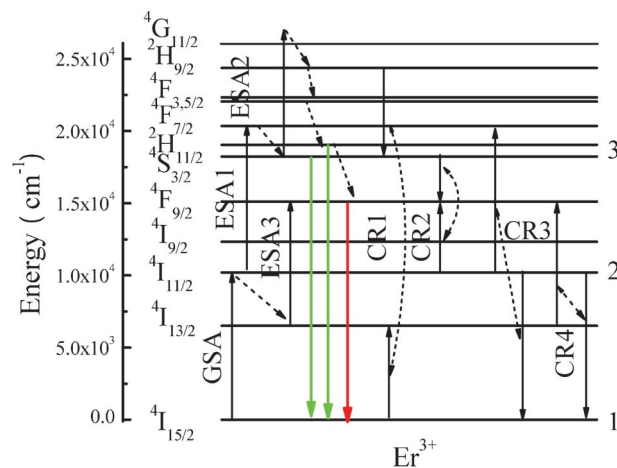


Fig. 3 The UC mechanism as well as the proposed CR processes under 980 nm excitation.

GSA and ESA1, the Er³⁺ ions at the $^4S_{3/2}$ state absorb a third laser photon, and then are excited to the $^4G_{11/2}$ state (ESA2: $^4S_{3/2} + \text{a 980 nm photon} \rightarrow ^4G_{11/2}$). Nonradiatively relaxing from the $^4G_{11/2}$ state is a contribution to populate the green emitting $^4S_{3/2}/^2H_{11/2}$ states and the red emitting $^4F_{9/2}$ state. The metastable $^2H_{9/2}$ state, which is populated *via* the nonradiative relaxation from $^4G_{11/2}$ state, has enough time to allow the CR1 process ($^2H_{9/2} + ^4I_{11/2} \rightarrow ^4S_{3/2} + ^4I_{15/2}$) to occur. The enhanced population of $^4S_{3/2}$ state results in the occurrence of the CR2 process ($^4S_{3/2} + ^4I_{11/2} \rightarrow ^4F_{9/2} + ^4F_{9/2}$). It is clear that the CR1 and CR2 processes result in an increasing population of the $^4F_{9/2}$ state. According to the pump power dependences (Fig. 2), the CR1 and CR2 processes only occur in the Er:NSLN crystal due to the three-photon process. The overall result is a drastic enhancement of red UC emission in Er:NSLN crystal, in agreement with the experimental results shown in Fig. 1.

The decreased slope value $n = 1$ with the increasing pump power is attributed to the competition of linear decay and UC processes,^{29,24} which can be explained as follows. The energy level of Er³⁺ ions are simply considered as a three-level system, and the ground $^4I_{15/2}$ state, the intermediate $^4I_{11/2}$ state and the green emitting $^4S_{3/2}/^2H_{11/2}$ states are named as 1, 2 and 3, respectively. GSA is contribution to the population of state 2. It assumes that the state 3 is populated only by ESA or energy transfer upconversion (ETU). The sensitization effect caused by the sensitizer and the excited state bleaching are excluded here. The rate equations can be written as:

$$dN_2/dt = \rho_p \sigma_1 N_1 - \rho_p \sigma_2 N_2 \text{ (or } 2W_2 N_2^2) - A_2 N_2 \quad (2)$$

$$dN_3/dt = \rho_p \sigma_2 N_2 \text{ (or } W_2 N_2^2) - A_3 N_3 \quad (3)$$

where the term $\rho_p \sigma_2 N_2$ means the state 3 (the green emitting $^4S_{3/2}/^2H_{11/2}$ states) is populated *via* ESA, or the term $W_2 N_2^2$ indicates that the state 3 is achieved by ETU process; σ_i is the absorption cross section, A_i is the spontaneous emission constant, W_i is the energy transfer constant, and ρ_p is the

pump rate and defined as:

$$\rho_p = \frac{\lambda_p P}{hc\pi w_p^2} \quad (4)$$

where λ_p , P and w_p are the excited wavelength, the incident pump power and the pump radius, respectively; h is Planck's constant, and c is the speed of light. Under the steady-state excitation, as for the ESA process, eqn (2) and (3) can be simplified as follows:

$$\rho_p \sigma_1 N_1 = \rho_p \sigma_2 N_2 + A_2 N_2 \quad (5)$$

$$A_3 N_3 = \rho_p \sigma_2 N_2 \quad (6)$$

The ESA term $\rho_p \sigma_2 N_2$ in eqn (5) can be neglected when state 2 linearly decays primarily to the ground state 1, yielding luminescence. Then, there are the following conclusions $N_2 = \rho_p \sigma_1 N_1 / A_2 \propto \rho_p \propto P$ obtained from eqn (5) and $N_3 = \rho_p \sigma_2 N_2 / A_3 \propto \rho_p N_2 \propto \rho_p^2 \propto P^2$ obtained from eqn (6). In contrast, as the ESA process plays an important role in state 2, the linear decay term ($A_2 N_2$) can be neglected in eqn (5). We can gain these relations: $N_2 = \rho_p \sigma_1 N_1 / \rho_p \sigma_2 \propto \rho_p^0 \propto P^0$ from eqn (5) and $N_3 = \rho_p \sigma_2 N_2 / A_3 \propto \rho_p N_2 \propto \rho_p \propto P$ from eqn (6).

Similarly, when the state is populated *via* ETU process, eqn (2) and (3) can be simplified under the steady-state excitation:

$$\rho_p \sigma_1 N_1 = 2W_2 N_2^2 + A_2 N_2 \quad (7)$$

$$W_2 N_2^2 = A_3 N_3 \quad (8)$$

As the linearly decay process from the state 2 to the ground state 1 (luminescence) is dominant, the ETU term ($W_2 N_2^2$) in eqn (7) are neglected. The conclusions $N_2 = \rho_p \sigma_1 N_1 / A_2 \propto \rho_p \propto P$ and $N_3 = W_2 N_2^2 / A_3 \propto N_2^2 \propto \rho_p^2 \propto P^2$ are obtained from eqn (7) and (8), respectively. The linearly decay term ($A_2 N_2$) is not considered at the primary ETU process of state 2, and then the relationships $N_2^2 = \rho_p \sigma_1 N_1 / 2W_2 \propto \rho_p \propto P$ and $N_3 = W_2 N_2^2 / A_3 \propto N_2^2 \propto P$ are obtained from eqn (7) and (8), respectively. Accordingly, the slope value $n = 1$ indicates that the linear decay process is the primary one for the depletion of the intermediate excited states (${}^4I_{11/2}$) in Er:NSLN and Er:CLN crystals at the high pump power.

Fig. 4 displays the UV-vis-near infrared absorption spectra of Er:NSLN and Er:CLN crystals in the range from 300 to 1650 nm. The absorption bands centered at 368, 381, 410, 453, 492, 525, 550, 660, 980 and 1540 nm are attributed to the transitions from the ground ${}^4I_{15/2}$ state to the ${}^4G_{9/2}$, ${}^4G_{11/2}$, ${}^2H_{9/2}$, ${}^4F_{3/2}$, ${}^4F_{7/2}$, ${}^2H_{11/2}$, ${}^4S_{3/2}$, ${}^4F_{9/2}$, ${}^4I_{11/2}$ and ${}^4I_{13/2}$ states of Er^{3+} ion, respectively. The segregation coefficients of Er^{3+} ion are measured to calculate the J–O intensity parameters, which are about 1.47 and 1.41 for Er:CLN and Er:NSLN crystals, respectively. Accordingly, the concentrations of Er^{3+} ion in the crystal are obtained to be $8.33 \times 10^{20} \text{ cm}^{-3}$ and $7.96 \times 10^{20} \text{ cm}^{-3}$ in Er:CLN and Er:NSLN crystals, respectively.

The J–O intensity parameters of Er:NSLN crystal can be obtained based on the J–O theory, and the corresponding calculated procedures have been reported earlier.^{30–32} The

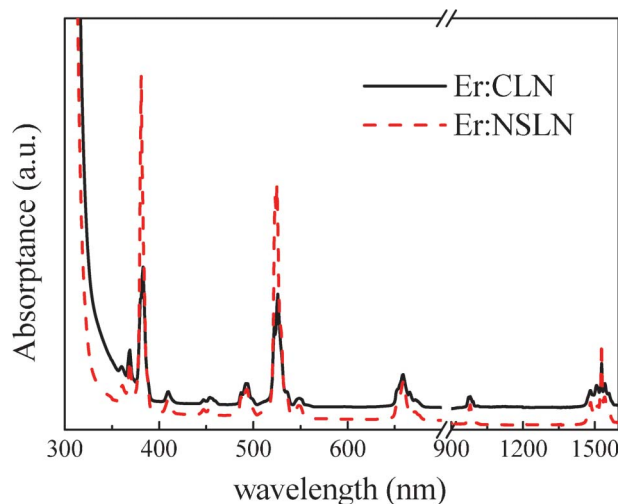


Fig. 4 UV-vis-near infrared absorption spectra of Er:NSLN and Er:CLN crystals.

value of the root mean-square deviation (δ_{rms}) is calculated to be 70×10^{-8} for Er:NSLN crystal, which is similar to that in Er (1 mol%):LiNbO₃ crystal (31×10^{-8}) reported by J. Amin,³³ indicating that the fitting results here may be credible. The J–O intensity parameters are $\Omega_2 = 9.17 \times 10^{-20} \text{ cm}^2$, $\Omega_4 = 2.47 \times 10^{-20} \text{ cm}^2$ and $\Omega_6 = 1.00 \times 10^{-20} \text{ cm}^2$ for Er:NSLN crystal. It can be found from our previous work that the J–O intensity parameters are $\Omega_2 = 3.89 \times 10^{-20} \text{ cm}^2$, $\Omega_4 = 2.20 \times 10^{-20} \text{ cm}^2$ and $\Omega_6 = 0.56 \times 10^{-20} \text{ cm}^2$ for Er (3 mol%):CLN crystal.³⁴ The value of Ω_2 in Er:NSLN is larger than that in Er:CLN crystal, which may be attributed to the high absorption of the hypersensitive transitions of ${}^4I_{15/2} \rightarrow {}^2H_{11/2}/{}^4G_{11/2}$. This is because that Ω_2 is closely related to the hypersensitive transitions which are sensitive to the variation of local structure around the Er^{3+} ions. The intensity parameters Ω_4 and Ω_6 are associated with the bulk properties and rigidity of the samples. The important parameter sum of Ω ($\Omega_{\text{sum}} = \Omega_2 + \Omega_4 + \Omega_6$) equates to the transition strengths. The value of Ω_{sum} ($\Omega_{\text{sum}} = 12.64 \times 10^{-20} \text{ cm}^2$) in Er:NSLN is larger than that in Er:CLN ($\Omega_{\text{sum}} = 6.65 \times 10^{-20} \text{ cm}^2$), suggesting that the Er:NSLN crystal could be considered as a potential material for future luminescent layer application in solar cells.

Accurate absorption and emission cross-sections are essential to the quantitative understanding of devices as well as the identification of improved active media. McCumber theory is a generalization of the original Einstein *A* and *B* coefficients approach and can be applied to the broadband transitions between the Stark manifolds of a rare-earth ion. Assuming that the time taken to establish a thermal distribution within each manifold is short compared with the lifetime of the manifold. Firstly, the emission cross-section (σ_{em}) could be evaluated from the green and red UC emission spectra (Fig. 1), and the calculated equation is expressed as:^{35,36}

$$\sigma_{em}(\lambda) = \frac{\lambda^5 A_{rad} I(\lambda)}{8\pi c n^2 \int \lambda I(\lambda) d\lambda} \quad (9)$$

where λ is the wavelength of the emission peak, $I(\lambda)$ is the fluorescent intensity at wavelength λ , c is the speed of light, and A_{rad} is the spontaneous transition rate, which can be calculated by the following equations:

$$A_{rad}(J \rightarrow J') = \frac{4\pi^2 e^2 n}{3h(2J+1)\lambda^3} \times \left[\frac{16\pi^2 (n^2 + 2)^2}{9} \sum_{t=2,4,6} \Omega_t |\langle SLJ || U^{(t)} || S'L'J' \rangle|^2 + \frac{n^2 h^2}{m^2 c^2} |\langle SLJ || \vec{L} + 2\vec{S} || S'L'J' \rangle|^2 \right] \quad (10)$$

where the values of Ω_t ($t = 2, 4$ and 6) have been obtained by J-O theory, J and J' represent an initial and a final manifold in the theoretical transition strength of Er^{3+} ion, respectively; n is the refractive indices of LiNbO_3 crystal; λ is barycentre wavelength at a given absorption band, m , c and h are the mass of the electron, light speed in a vacuum and Planck's constant, respectively; The term $|\langle SLJ || U^{(t)} || S'L'J' \rangle|^2$ is the doubly reduced matrix elements of the unit-tensor operator $U^{(t)}$; The term $|\langle SLJ || \vec{L} + 2\vec{S} || S'L'J' \rangle|^2$ is calculated based on the spin angular momentum (S), orbital angular momentum (L) and the total angular momentum quantum number (J), and the corresponding calculated formulae are given in ref. 37. Table 1 shows the calculated values of spontaneous transition rate (A_{rad}) for the transition from the $^4S_{3/2}$, $^2H_{11/2}$ and $^4F_{9/2}$ states to the ground $^4I_{15/2}$ state.

As for the $^4S_{3/2}/^2H_{11/2} \rightarrow ^4I_{15/2}$ transition, the two thermalized states $^4S_{3/2}$ and $^2H_{11/2}$ are named as l and u , respectively. The effective radiative rate A_{eff} for the thermalized states $^4S_{3/2}$ (l) and $^2H_{11/2}$ (u) is calculated and listed in Table 1, and the equation is given by:

$$A_{eff} = \frac{\exp(-\frac{\epsilon_{ul}}{kT}) A_{ug} + A_{lg}}{1 + \exp(-\frac{\epsilon_{ul}}{kT})} \quad (11)$$

where k and T are the Boltzmann's constant and the temperature, respectively; A_{ug} and A_{lg} represent the radiative rate from the upper state $^2H_{11/2}$ and the lower state $^4S_{3/2}$ to the ground state $^4I_{15/2}$, respectively; ϵ_{ul} , the excitation energy of the transition between the two thermalized states, are 803.4 and 759.3 cm^{-1} , respectively, for Er:CLN and Er:NSLN crystals. Consequently, based on eqn (9), the emission cross-section (σ_{em}) spectra of the green and red UC emissions in Er:CLN and

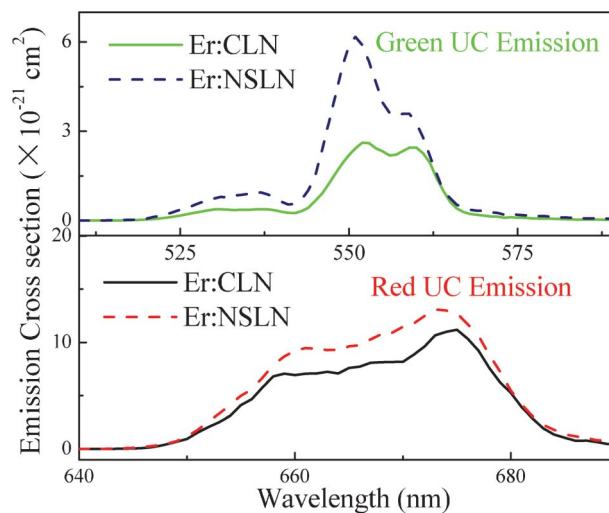


Fig. 5 The emission cross section of the green and red UC emission in Er:NSLN and Er:CLN crystals.

Er:NSLN crystals are gained and displayed in Fig. 5. It can be seen that the increasing $[\text{Li}]/[\text{Nb}]$ ratio leads to the enhancement of the emission cross-sections for the green and red UC emissions in NSLN crystal, favoring visible luminescence re-absorbed by the solar cells.

The relation between absorption cross-section (σ_{abs}) and the corresponding emission cross-section (σ_{em}) can be determined by the McCumber relation:^{21,38}

$$\sigma_{abs}(\lambda) = \sigma_{em}(\lambda) \exp\left[\frac{h\nu - \epsilon_T}{kT}\right] \quad (12)$$

where $\nu = c/\lambda$, c and λ are the light speed and the wavelength, respectively, h is the Planck's constant, k is Boltzmann's constant, T is the absolute temperature, and ϵ_T is a temperature-dependent effective excitation energy between the two manifolds and can be evaluated by using the following equations:²⁰

$$\frac{N_2}{N_1} = \exp\left(-\frac{\epsilon_T}{kT}\right) \quad (13)$$

where N_1 and N_2 are the equilibrium populations of the transition lower and upper states, respectively.

In the case of the $^4S_{3/2}/^2H_{11/2} \rightarrow ^4I_{15/2}$ transition, ϵ_T , the effective excitation energy for the two thermalized manifolds, is calculated according to the following expression:

$$\frac{N_l}{N_g} = \exp\left(-\frac{\Delta E_{lg}}{kT}\right) \frac{1 - \exp\left(-\frac{\delta E_g}{kT}\right)}{1 - \exp\left(-\frac{g_g \delta E_g}{kT}\right)} \times \left[\frac{1 - \exp\left(-\frac{g_l \delta E_l}{kT}\right)}{1 - \exp\left(-\frac{\delta E_l}{kT}\right)} + \frac{\exp\left(-\frac{g_l \delta E_l}{kT}\right)}{1 - \exp\left(-\frac{\Delta E_{ul} - g_l \delta E_l}{kT}\right)} \right] \times \frac{1 - \exp\left(-\frac{g_u \delta E_u}{kT}\right)}{1 - \exp\left(-\frac{\delta E_u}{kT}\right)} \quad (14)$$

Table 1 The spontaneous transition rate (A_{rad}) in Er:NSLN and Er:CLN crystals

Transitions	Parameters (s^{-1})	Er:CLN	Er:NSLN
$^4S_{3/2} + ^2H_{11/2} \rightarrow ^4I_{15/2}$	A_{ug}	20306	41642
	A_{lg}	1736	3136
	A_{eff}	2064	3981
$^4F_{9/2} \rightarrow ^4I_{15/2}$	A_{eff}	4360	5441

Table 2 Parameters for calculations of absorption cross-section in Er:NSLN and Er:CLN crystals

Transitions	Parameters	Er:CLN	Er:NSLN
${}^4S_{3/2} + {}^2H_{11/2} \rightarrow {}^4I_{15/2}$	δE_{ig} (cm ⁻¹)	18171.9	18198.4
	ΔE_{ul} (cm ⁻¹)	803.4	759.3
	δE_i (cm ⁻¹)	63.0	49.8
$u = {}^2H_{11/2}$	δE_u (cm ⁻¹)	48.1	36.9
	δE_g (cm ⁻¹)	45.0	64.6
$l = {}^4S_{3/2}$	$1/\ell_T$ (nm)	545.3	546.0
$g = {}^4I_{15/2}$	ΔE_{ba} (cm ⁻¹)	14867.0	14867.0
${}^4F_{9/2} \rightarrow {}^4I_{15/2}$	E_a (cm ⁻¹)	96.4	89.9
	E_b (cm ⁻¹)	54.5	57.15
$a = {}^4F_{9/2}$	$1/\ell_T$ (nm)	675.1	674.5
$b = {}^4I_{15/2}$			

where the ground state ${}^4I_{15/2}$ is defined as g; δE_{ij} represents the energy separation between the states i and j (i, j = l, u and g), δE_i is the component spacing for the state i (i = l, u and g), and g_i is the degeneracy of state. Here, g_u , g_l and g_g , representing the degeneracy of states ${}^2H_{11/2}$, ${}^4S_{3/2}$ and ${}^4I_{15/2}$, are equal to be 6, 2 and 8, respectively.

The red emitting ${}^4F_{9/2}$ state and the ground ${}^4I_{15/2}$ state are denominated as b and a, respectively, and then the population rate $\left(\frac{N_b}{N_a}\right)$ can be expressed as:

$$\frac{N_b}{N_a} = \exp\left(\frac{-\Delta E_{ba}}{kT}\right) \frac{1 - \exp(-\delta E_a/kT)}{1 - \exp(-\delta E_b/kT)} \frac{1 - \exp(-g_b \delta E_b/kT)}{1 - \exp(-g_a \delta E_a/kT)} \quad (15)$$

where δE_{ba} represents the energy separation between the state ${}^4F_{9/2}$ and the ground state ${}^4I_{15/2}$, δE_b and δE_a are the component spacing for ${}^4F_{9/2}$ and ${}^4I_{15/2}$ states, respectively. The degeneracy of ${}^4F_{9/2}$ (g_b) and ${}^4I_{15/2}$ (g_a) are 5 and 8, respectively. These parameters used to calculate the absorption cross-section (σ_{abs}) have been obtained from Fig. 1 and listed in Table 2. Therefore, according to the combination of eqn (13) with eqn (14) or eqn (15), the values of

ℓ_T for the ${}^4S_{3/2}/{}^2H_{11/2} \rightarrow {}^4I_{15/2}$ and ${}^4F_{9/2} \rightarrow {}^4I_{15/2}$ transitions are determined and also shown in Table 2. The absorption cross-section spectra of the green and red UC emissions in Er:NSLN and Er:CLN crystals are obtained via eqn (12) and illustrated in Fig. 6. It is obvious that a drastically enhanced absorption cross-section of green emission is observed in the Er:NSLN crystal.

4. Conclusion

In conclusion, the green and red UC emission spectra of the near-stoichiometric LiNbO₃ crystal heavily doped with Er³⁺ ions grown by the Czochralski technique are investigated. The enhanced intensities of the green and red UC emissions imply that Er:NSLN converts successfully the near-infrared wavelength into the visible UC emission re-absorbed by the solar cells. Studies on the UC mechanism show that the green emitting ${}^4S_{3/2}/{}^2H_{11/2}$ states and red emitting ${}^4F_{9/2}$ state are populated by the three-photon process at the low pump power, and the cross relaxation processes ${}^2H_{9/2} + {}^4I_{11/2} \rightarrow {}^4S_{3/2} + {}^4I_{15/2}$ and ${}^4S_{3/2} + {}^4I_{11/2} \rightarrow {}^4F_{9/2} + {}^4F_{9/2}$ are contribution to the enhanced red UC emission in the Er:NSLN crystal. At the high pump power, the green emission exhibits the saturated UC process. A procedure based on McCumber theory is used to understand the emission and absorption cross-sections for the ${}^4F_{9/2} \rightarrow {}^4I_{15/2}$ transition and the thermalized ${}^2H_{11/2}/{}^4S_{3/2} \rightarrow {}^4I_{15/2}$ transitions of the Er³⁺ ion. Experimental results indicate that as the [Li]/[Nb] ratio is equal to 1, the absorption and emission cross-sections for green and red UC emission increase, indicating that Er:NSLN could be considered as a potential luminescent layer for solar cells.

Acknowledgements

We are grateful to National Natural Science Foundation of China (No. 10732100, 11232015, 11072271 and 10972239) and the China Postdoctoral Science Foundation (No.:2012M521640).

References

- O. Morton, Solar energy: A new day dawning? Silicon Valley sunrise, *Nature*, 2006, **443**, 19–22.
- B. M. van der Ende, L. Aarts and A. Meijerink, Lanthanide ions as spectral converters for solar cells, *Phys. Chem. Chem. Phys.*, 2009, **11**, 11081–11095.
- V. D. Rodríguez, V. K. Tikhomirov, J. Méndez-Ramos, A. C. Yanes and V. V. Moshchalkov, Towards broad range and highly efficient down-conversion of solar spectrum by Er³⁺-Yb³⁺ co-doped nano-structured glass-ceramics, *Sol. Energy Mater. Sol. Cells*, 2010, **94**, 1612–1617.
- Y. Y. Cheng, B. Fückel, R. W. MacQueen, T. Khoury Raphaël, G. C. R. Clady, T. F. Schulze, N. J. Ekins-Daukes, M. J. Crossley, B. Stannowski, K. Lips and T. W. Schmidt, Improving the light-harvesting of amorphous silicon solar cells with photochemical upconversion, *Energy Environ. Sci.*, 2012, **5**, 6953–6959.

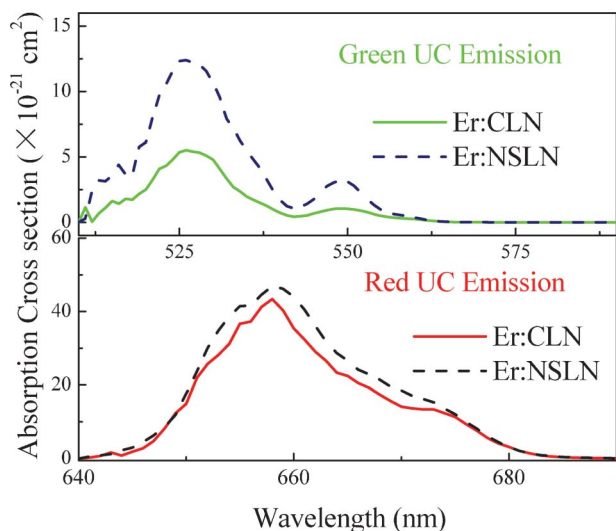


Fig. 6 The absorption cross-section of the green and red UC emissions in Er:NSLN and Er:CLN crystals.

- 5 A. Shalav, B. S. Richards, T. Trupke, K. W. Krämer and H. U. Güdel, Application of $\text{NaYF}_4:\text{Er}^{3+}$ up-converting phosphors for enhanced near-infrared silicon solar cell response, *Appl. Phys. Lett.*, 2005, **86**, 013505–013505-3.
- 6 X. Y. Huang, S. Y. Han, W. Huang and X. G. Liu, Enhancing solar cell efficiency: the search for luminescent materials as spectral converters, *Chem. Soc. Rev.*, 2013, **42**, 173–201.
- 7 D. Q. Chen, Y. S. Wang, K. L. Zheng, T. L. Guo, Y. L. Yu and P. Huang, Bright upconversion white light emission in transparent glass ceramic embedding $\text{Tm}^{3+}/\text{Er}^{3+}/\text{Yb}^{3+}:\beta\text{-YF}_3$ nanocrystals, *Appl. Phys. Lett.*, 2007, **91**, 251903-1–251903-3.
- 8 H. Q. Wang, M. Batentschuk, A. Osvet, L. Pinna and C. J. Brabec, Rare-Earth Ion Doped Up-Conversion Materials for Photovoltaic Applications, *Adv. Mater.*, 2011, **23**, 2675–2680.
- 9 J. C. Goldschmidt, S. Fischer, P. Löper, K. W. Krämer, D. Biner, M. Hermle and S. W. Glunz, Experimental analysis of upconversion with both coherent monochromatic irradiation and broad spectrum illumination, *Sol. Energy Mater. Sol. Cells*, 2011, **95**, 1960–1963.
- 10 A. Shalav, B. S. Richards and M. A. Green, Luminescent layers for enhanced silicon solar cell performance: Up-conversion, *Sol. Energy Mater. Sol. Cells*, 2007, **91**, 829–842.
- 11 V. K. Tikhomirov, V. D. Rodríguez, J. Méndez-Ramos, J. del-Castillo, D. Kirilenko, G. Van Tendeloo and V. V. Moshchalkov, Optimizing Er/Yb ratio and content in Er-Yb co-doped glass-ceramics for enhancement of the up- and down-conversion luminescence, *Sol. Energy Mater. Sol. Cells*, 2012, **100**, 209–215.
- 12 F. Lahoz, C. Pérez-Rodríguez, S. E. Hernández, I. R. Martín, V. Lavín and U. R. Rodríguez-Mendoza, Upconversion mechanisms in rare-earth doped glasses to improve the efficiency of silicon solar cells, *Sol. Energy Mater. Sol. Cells*, 2011, **95**, 1671–1677.
- 13 J. de Wild, J. K. Rath, A. Meijerink, W. G. J. H. M. van Sark and R. E. I. Schropp, Enhanced near-infrared response of a-Si:H solar cells with $\beta\text{-NaYF}_4:\text{Yb}^{3+}(18\%), \text{Er}^{3+}(2\%)$ upconversion phosphors, *Sol. Energy Mater. Sol. Cells*, 2010, **94**, 2395–2398.
- 14 D. Janner, D. Tulli, M. García-Granda, M. Belmonte and V. Pruneri, Micro-structured integrated electro-optic LiNbO_3 modulators, *Laser Photonics Rev.*, 2009, **3**, 301–313.
- 15 J. B. Gruber, D. K. Sardar, R. M. Yow, B. Zandi and E. P. Kokanyan, Modeling the crystal-field splitting of the energy levels of Er^{3+} in charge-compensated sites in lithium niobate, *Phys. Rev. B: Condens. Matter Mater. Phys.*, 2004, **69**, 195103–195112.
- 16 L. H. Slooff, A. van Blaaderen, A. Polman, G. A. Hebbink, S. I. Klink, F. C. J. M. Van Veggel, D. N. Reinhoudt and J. W. Hofstraat, Rare-earth doped polymers for planar optical amplifiers, *J. Appl. Phys.*, 2002, **91**, 3955–3980.
- 17 P. Lerner, C. Legras and J. P. Dumas, *Stoichiométrie des monocristaux de métaniobate de lithium*, *J. Cryst. Growth*, 1968, **3–4**, 231–235.
- 18 Y. Furukawa, K. Kitamura, S. Takekawa, A. Miyamoto, M. Terao and N. Suda, Photorefractive in LiNbO_3 as a function of $[\text{Li}]/[\text{Nb}]$ and MgO concentrations, *Appl. Phys. Lett.*, 2000, **77**, 2494–2496.
- 19 M. Á. Rebolledo, J. A. Vallés and S. Setién, *In situ* measurement of polarization-resolved emission and absorption cross sections of Er-doped $\text{Ti}:\text{LiNbO}_3$ waveguides, *J. Opt. Soc. Am. B*, 2002, **19**, 1516–1520.
- 20 J. A. Lázaro, J. A. Vallés and M. A. Rebolledo, Determination of emission and absorption cross sections of Er^{3+} in $\text{Ti}:\text{LiNbO}_3$ waveguides from transversal fluorescence spectra, *Pure Appl. Opt.*, 1998, **7**, 1363–1371.
- 21 J. A. Lázaro, J. A. Vallés and M. A. Rebolledo, In Situ Measurement of Absorption and Emission Cross Sections in Er-Doped Waveguides for Transitions Involving Thermalized States, *IEEE J. Quantum Electron.*, 1999, **35**, 827–831.
- 22 F. Liu, E. Ma, D. Q. Chen, Y. L. Yu and Y. S. Wang, Tunable Red-Green Upconversion Luminescence in Novel Transparent Glass Ceramics Containing $\text{Er}:\text{NaYF}_4$ Nanocrystals, *J. Phys. Chem. B*, 2006, **110**, 20843–20846.
- 23 F. Pandozzi, F. Vetrone, J. C. Boyer, R. Naccache, J. A. Capobianco, A. Speghini and M. Bettinelli, A Spectroscopic Analysis of Blue and Ultraviolet Upconverted Emissions from $\text{Gd}_3\text{Ga}_5\text{O}_{12}:\text{Tm}^{3+}, \text{Yb}^{3+}$ Nanocrystals, *J. Phys. Chem. B*, 2005, **109**, 17400–17405.
- 24 S. K. Singh, K. Kumar and S. B. Rai, Multifunctional $\text{Er}^{3+}\text{-Yb}^{3+}$ codoped Gd_2O_3 nanocrystalline phosphor synthesized through optimized combustion route, *Appl. Phys. B: Lasers Opt.*, 2008, **94**, 165–173.
- 25 A. H. Li, Z. R. Zheng, T. Q. Lü, L. Sun, W. L. Liu and W. Z. Wu, Influence of MgO codoping on the optical properties of Er^{3+} doped near-stoichiometric LiNbO_3 , *Appl. Phys. B: Lasers Opt.*, 2009, **98**, 149–158.
- 26 L. Sun, C. H. Yang, A. H. Li, Y. H. Xu and L. C. Zhao, In/Er-codoped LiNbO_3 crystals with enhanced 1.5 μm emission and suppressed upconversion emission, *J. APPL. Phys.*, 2009, **105**, 043512-1–043512-6.
- 27 G. C. Jones and S. N. Houde-Walter, Upconversion mechanisms in an erbium-doped transparent glass ceramic, *J. Opt. Soc. Am. B*, 2005, **22**, 825–830.
- 28 A. Patra, C. S. Friend, R. Kapoor and P. N. Prasad, Fluorescence Upconversion Properties of Er^{3+} -Doped TiO_2 and BaTiO_3 Nanocrystallites, *Chem. Mater.*, 2003, **15**, 3650–3655.
- 29 M. Pollnau, D. R. Gamelin, S. R. Lüthi, H. U. Güdel and M. P. Hehlen, Power dependence of upconversion luminescence in lanthanide and transition-metal-ion systems, *Phys. Rev. B: Condens. Matter*, 2000, **61**, 3337–3346.
- 30 A. Li, L. Sun, Z. Zheng, Q. Lü, W. Wu, W. Liu, Y. Yang and T. Lü, Spectroscopic properties of Er^{3+} ions in LiNbO_3 crystals codoped with HfO_2 , *Appl. Phys. B: Lasers Opt.*, 2007, **90**, 29–34.
- 31 M. D. Shinn, W. A. Sibley, M. G. Drexhage and R. N. Brown, Optical transitions of Er^{3+} ions in fluorozirconate glass, *Phys. Rev. B*, 1983, **27**, 6635–6648.
- 32 M. P. Hehlen, N. J. Cockroft, T. R. Gosnell and A. J. Bruce, Spectroscopic properties of Er^{3+} - and Yb^{3+} -doped soda-lime silicate and aluminosilicate glasses, *Phys. Rev. B: Condens. Matter*, 1997, **56**, 9302–9318.
- 33 J. Amin, B. Dussardier, T. Schweizer and M. Hempstead, Spectroscopic analysis of Er^{3+} transitions in lithium niobate, *J. Lumin.*, 1996, **69**, 17–26.
- 34 Y. N. Qian, R. Wang, B. Wang, C. Xu, L. L. Xing and Y. L. Xu, Defect structures and optical characteristics of Er^{3+} ion in $\text{Er}:\text{LiNbO}_3$ crystals, *J. Mol. Struct.*, 2013, **1035**, 101–108.

- 35 J. F. Tang, Y. J. Chen, Y. F. Lin, X. H. Gong, J. H. Huang, Z. D. Luo and Y. D. Huang, Tm³⁺/Ho³⁺ co-doped LiGd(MoO₄)₂ crystal as laser gain medium around 2.0 μm, *Opt. Mater. Express*, 2012, **2**, 1064–1075.
- 36 S. Balaji, A. D. Sontakke, R. Sen and A. Kalyandurg, Efficient ~2.0 μm emission from Ho³⁺ doped tellurite glass sensitized by Yb³⁺ ions: Judd–Ofelt analysis and energy transfer mechanism, *Opt. Mater. Express*, 2011, **1**, 138–150.
- 37 M. J. Weber, Probabilities for Radiative and Nonradiative Decay of Er³⁺ in LaF₃, *Phys. Rev.*, 1967, **157**, 262–272.
- 38 D. L. Zhang, J. Gao, J. A. Vallés, C. Xu, L. Sun, Y. H. Xu and E. Y. B. Pun, Emission and Absorption Cross-Sections of Mg/Er-Codoped Near-Stoichiometric LiNbO₃ Crystals, *IEEE J. Quantum Electron.*, 2010, **46**, 1332–1341.